1 **Diagnosing CO$_2$ fluxes in the upwelling system off the Oregon-California coast**

2 Zhimian Cao[1†], Minhan Dai[1]*, Wiley Evans[2,3], Jianping Gan[4], Richard Feely[2]

3 [1]State Key Laboratory of Marine Environmental Science, Xiamen University, Xiamen, China

4 [2]Pacific Marine Environmental Laboratory, National Oceanic and Atmospheric Administration,

5 Seattle, Washington, USA

6 [3]Ocean Acidification Research Center, School of Fisheries and Ocean Sciences, University of

7 Alaska Fairbanks, Fairbanks, Alaska, USA

8 [4]Division of Environment and Department of Mathematics, Hong Kong University of Science

9 and Technology, Kowloon, Hong Kong, China

10 [†]Present address: GEOMAR | Helmholtz Center for Ocean Research Kiel, Kiel, Germany

11

12 *Corresponding author:

13 Dr. Minhan Dai

14 State Key Laboratory of Marine Environmental Science

15 Xiamen University

16 Xiang'an District

17 Xiamen 361102, China

18 Phone: +86-592-2182132

19 Fax: +86-592-2184101

20 E-mail: mdai@xmu.edu.cn

Abstract

It is generally known that the interplay between the carbon and nutrients supplied from subsurface waters via biological metabolism determines the CO_2 fluxes in upwelling systems. However, quantificational assessment of such interplay is difficult because of the dynamic nature of both upwelling circulation and the associated biogeochemistry. We recently proposed a new framework, the Ocean-dominated Margin (OceMar), for semi-quantitatively diagnosing the CO_2 source/sink nature of an ocean margin over a given period of time, highlighting that the relative consumption between carbon and nutrients determines if carbon is in excess (i.e., CO_2 source) or in deficit (i.e., CO_2 sink) in the upper waters of ocean margins relative to their off-site inputs from the adjacent open ocean. In the present study, such a diagnostic approach based upon both couplings of physics-biogeochemistry and carbon-nutrients was applied to resolve the CO_2 fluxes in the well-known upwelling system in the US west coast off Oregon and northern California, using data collected along three cross-shelf transects from the inner shelf to the open basin in spring/early summer 2007. Through examining the biological consumption on top of the water mass mixing revealed by the total alkalinity-salinity relationship, we successfully predicted and semi-analytically resolved the CO_2 fluxes showing strong uptake from the atmosphere beyond the nearshore regions. This CO_2 sink nature primarily resulted from the higher utilization of nutrients relative to dissolved inorganic carbon (DIC) based on their concurrent inputs from the depth. On the other hand, the biological responses to intensified upwelling were minor in nearshore waters off the Oregon-California coast, where significant CO_2 outgassing was observed during the sampling period and resolving CO_2 fluxes could be simplified without considering DIC/nutrient consumption, i.e., decoupling between upwelling and biological consumption. We reasoned that coupling physics and biogeochemistry in the OceMar model

44 would assume a steady state with balanced DIC and nutrients via both physical transport and

45 biological alterations in comparable timescales.

46

47 **Keywords**

1 Introduction

The contemporary coastal ocean, characterized by high primary productivity due primarily to the abundant nutrient inputs from both river plumes and coastal upwelling, is generally seen as a significant CO_2 sink at the global scale (Borges et al., 2005; Cai et al., 2006; Chen and Borges, 2009; Laruelle et al., 2010; Borges, 2011; Cai, 2011; Dai et al., 2013). However, mechanistic understanding of the coastal ocean carbon cycle remains limited, leading to the unanswered question of why some coastal systems are sources while others are sinks of atmospheric CO_2 in a given timescale. We recently proposed a new framework, the Ocean-dominated Margin (OceMar), for better shaping the concept of a coastal ocean carbon study (Dai et al., 2013). This framework highlights the importance of the boundary process between the open ocean and the ocean margin, and proposes a semi-analytical diagnostic approach to resolve sea-air CO_2 fluxes over a given period of time. The approach invokes an establishment of the water mass mixing scheme in order to define the physical transport, or the conservative portion of carbon and nutrients from the adjacent open ocean; and the constraint of the biogeochemical alteration of these non-local inputs in the upper waters of ocean margins. The water mass mixing scheme is typically revealed using conservative chemical tracers such as total alkalinity (TAlk) and/or dissolved calcium ions (Ca^{2+}) to bypass the identification of end-members associated with individual water masses that often possess high complexity in any given oceanic regime. The constraint of the biogeochemical alteration can then be estimated as the difference between the predicted values based on conservative mixing between end-members and the field measured values. The relative consumption between dissolved inorganic carbon (DIC) and nutrients determines if DIC is in excess or in deficit relative to the off-site input. Such excess DIC will eventually be released to the atmosphere through air-sea CO_2 exchange. Using two large

73 marginal seas, the South China Sea (SCS) and the Caribbean Sea (CS) as examples, we have

74 successfully predicted, via evaluating DIC and nutrient mass balance, the CO_2 outgassing that is

75 consistent with field observations (Dai et al., 2013). However, the OceMar concept and the

76 diagnostic approach have not been verified on upwelling systems that can be either sources (e.g.,

77 Friederich et al., 2002; Torres et al., 2003; Fransson et al., 2006) or sinks (e.g., Borges et al.,

78 2002; Santana-Casiano et al., 2009; Evans et al., 2012) of atmospheric CO_2. While it is generally

79 known that the interplay between the nutrients and DIC supplied from subsurface waters via

80 biological metabolism would determine the CO_2 fluxes in upwelling systems, quantificational

81 assessment of such interplay is difficult because of the dynamic nature of both upwelling

82 circulation and the associated biogeochemistry.

83   Our study therefore chose the upwelling system in the US west coast off Oregon and northern

84 California, to examine the CO_2 flux dynamics during the upwelling season through our proposed

85 mass balance approach associated with carbon/nutrient coupling. The system under study is part

86 of the eastern boundary current in the North Pacific (Fig. 1). While strong equatorward winds in

87 spring/summer drive offshore Ekman transport at the surface over the coastal waters, the carbon

88 and nutrient-rich deep water is transported shoreward and upward over the shelf to compensate

89 for the offshore transport in the surface layer (Huyer, 1983; Kosro et al., 1991; Allen et al., 1995;

90 Federiuk and Allen, 1995; Gan and Allen, 2002). Outcrops of waters from depths of 150-200 m

91 are frequently observed in the nearshore on the Oregon-California shelf, where the surface partial

92 pressure of CO_2 ($p$$CO_2$) can reach levels near 1000 µatm. This water is then transported seaward

93 and southward while the $p$$CO_2$ is drawn down by biological productivity, and can be down to

94 levels of ~200 µatm, far below the atmospheric $p$$CO_2$ value (Hales et al., 2005, 2012; Feely et al.,

95 2008; Evans et al., 2011). Such a dramatic decrease in seawater $p$$CO_2$ may be due to the fact that

96   the complete utilization of the preformed nutrients in upwelled waters exceeds their

97   corresponding net DIC consumption, leading to the area off Oregon and northern California

98   acting as a net sink of atmospheric CO_2 during the upwelling season (Hales et al., 2005, 2012).

99   On the other hand, Evans et al. (2011) suggest that the spring/early summer undersaturated pCO_2

100   conditions in some offshore areas result from non-local productivity associated with the

101   Columbia River (CR) plume, which transports ~77% of the total runoff from the western North

102   America to the Pacific Ocean (Hickey, 1989).

103   In this context, the Oregon-California shelf in the upwelling season can be a potential

104   OceMar-type system with the majority of DIC and nutrients in the upper layer originating from

105   the non-local deep waters in the subtropical gyre of the eastern North Pacific (eNP), though

106   riverine inputs might complicate the application of the OceMar framework. On the other hand,

107   the upper waters in offshore areas beyond the upwelling circulation on the Oregon-California

108   shelf would be largely fed by on-site deep waters via vertical mixing, with minor influence of the

109   CR plume.

110   **2 Study area and data source**

111   **2.1 California Current system and upwelling circulation**

112   The upwelling circulation off Oregon and northern California is linked with the eastern

113   boundary current, the California Current (CC) occupying the open basin of the eNP (Barth et al.,

114   2000). The CC is a broad and weak surface current (0-200 m) which carries low-

115   salinity/temperature water equatorward from the subarctic Pacific (Lynn and Simpson, 1987).

116   The deeper-lying California Undercurrent (CUC, 150-300 m), which has relatively high salinity

117   and temperature, originates in the eastern Equatorial Pacific and flows poleward inshore along

118   the west coast of North America (Thomson and Krassovski, 2010). The CC system is

119 characterized by coastal upwelling in spring/summer, during which waters primarily composed

120 of the CC are transported upward from the depths of 150-200 m towards the nearshore surface

121 off the Oregon-California coast (Castro et al., 2001).

122   Both field observations and modeling studies (Oke et al., 2002; Gan and Allen, 2005) show

123 that the upwelling circulation pattern in the study area differs significantly between north and

124 south of Newport (Fig. 1). North of Newport between 45.0 and 45.5°N with a relatively straight

125 coastline and narrow shelf, the along-shore uniform bottom topography generally results in

126 typical upwelling circulation with a southward coastal jet close to shore at Cascade Head (Fig. 1).

127 Over the central Oregon shelf between 43.5 and 45.0°N, the highly variable bottom topography

128 over Heceta Bank (Fig. 1) largely influences the upwelling circulation, leading to a complex

129 three-dimensional flow pattern with offshore shifting of the coastal jet and development of

130 northward flow inshore. At the coast along the southern part of Oregon and northern California

131 between 39.0 and 43.0°N, an enhancement of coastal upwelling, jet separation and eddy

132 formation are observed to be associated with interactions of the wind-forced coastal currents

133 with Cape Blanco (Fig. 1) (Barth et al., 1998; Gan and Allen, 2005, and references therein).

134 **2.2 Data source**

135   Our data sets were based on the online published carbonate system and nutrient data collected

136 along three transects off Oregon and northern California during the first North American Carbon

137 Program (NACP) West Coast Cruise in spring/early summer (May 11-June 14) 2007

138 (http://cdiac.ornl.gov/oceans/Coastal/NACP_West.html; Feely et al., 2008; Feely and Sabine,

139 2011). Transect 4 (stations 25-33 from nearshore to offshore) is located off Newport, Oregon.

140 Transect 5 (stations 41-35 from nearshore to offshore) is located off Crescent City near the

141 Oregon-California border. Transects 6 (stations 42-49 from nearshore to offshore) is located off

7

142   Cape Mendocino, California. The most offshore stations on all transects were located in the open

143   subtropical gyre of the eNP (Fig. 1).

3 Results and discussion

145   The region under study is highly dynamic potentially involving coastal upwelling, the CR

146   plume and pelagic waters mixed by various Pacific water masses (Hill and Wheeler, 2002).

147   Instead of accounting for all of the water masses contributing to the CC system, the mixing

148   scheme in the upper waters along the three transects was examined via the total alkalinity-

149   salinity (TAlk-Sal) relationship obtained during the sampling period so as to quantify the

150   conservative portion of DIC and nitrate (NO_3). The end-members were therefore identified under

151   this relationship, which might have experienced physical or biological alterations from their

152   original water masses such as the CR and the CC. Subsequently, the biologically consumed DIC

153   and NO_3 were quantified as the difference between their conservative values predicted from the

154   derived end-member mixing and the corresponding field measurements. Finally, the CO_2

155   source/sink nature of the upper waters off Oregon and northern California during the sampling

156   period was diagnosed via a mass balance approach by estimating the relative consumption

157   between DIC and NO_3 and a simple sensitivity analysis was performed to test the robustness of

158   the approach.

3.1 TAlk-Sal relationship

3.1.1 Through the entire water column off Oregon and northern California

161   Three generally linear relationships between TAlk and salinity were observed through the

162   entire water column along Transect 4 (Fig. 2a). The first one was for waters with salinity lower

163   than ~32.0 (corresponding to a depth of ~15-25 m), which were significantly influenced by the

164   CR plume. The second one was for waters composed primarily of the CC with salinity between

165 ~32.0 and ~33.9, including those immediately below the top buoyant layer at stations 26-32 and

166 the surface waters at the outermost station 33 (Fig. 1). The higher-end salinity value of ~33.9

167 corresponded to a depth range of ~75-175 m, composed possibly of the upwelled high-salinity

168 CUC waters. At station 27 (water depth ~170 m) for instance, salinity at depths of ~130 m and

169 ~160 m reached ~34.0 with TAlk values of ~2260 μmol kg^{-1}, which were even higher than those

170 of offshore waters at ~175 m (~2250 μmol kg^{-1}). These two data points were thus located on the

171 third linear relationship for waters with salinity higher than ~33.9, the slope of which became

172 much steeper, mainly reflecting the mixing between the approaching CUC and deep waters in the

173 subtropical gyre of the eNP (Fig. 2a).

174   All salinity values, including surface samples on Transects 5 and 6, were higher than 32.0 (Fig.

175 2b and 2c). With minor influence of the CR plume, the TAlk-Sal relationship displayed two

176 generally linear phases through the entire water column along both transects, while the

177 TAlk/salinity endpoints of each were comparable to those of the latter two observed on Transect

178 4. Note that the turning point with salinity of ~33.9 corresponded to a wider depth range of ~5-

179 175 m (Fig. 2b and 2c), resulting from the most intensive upwelling on Transects 5 and 6

180 bringing deep waters to the nearshore surface (Feely et al., 2008).

181   As suggested by the generally linear TAlk-Sal relationships, surface waters beyond the CR

182 plume and waters immediately below the top buoyant layer were directly linked to the

183 underlying waters to the depth of ~175 m. We thus took a closer look at the TAlk-Sal

184 relationship in the upper 175 m waters off Oregon and northern California.

185 **3.1.2 In the upper 175 m waters off Oregon and northern California**

186   In the upper 175 m waters along Transect 4, the linear regression for waters with salinity

187 lower than ~32.0 had an intercept of ~1200 μmol kg^{-1}. This value agreed well with the observed

188   TAlk of ~1000 μmol kg^{-1} in the main stream of the CR (Park et al., 1969b; Evans et al., 2013).

189   The other linear regression for waters with salinity between ~32.0 and ~33.9 had a smaller

190   intercept of ~500 μmol kg^{-1}, implying a smaller contribution from the CR plume (Fig. 3a).

191   Exceptions were observed at the shallowest station 25 (water depth ~50 m) and the deepest

192   station 33 (water depth ~2900 m). The TAlk-Sal relationship completely followed the second

193   phase for the upper 175 m waters at station 33 (Fig. 3a), suggesting a small fraction of the CR

194   plume even in the surface waters of this outermost station on Transect 4. On the other hand, data

195   points of the two variables were not well correlated through the entire water column of station 25

196   and fell off both regression lines (Fig. 3a). The water mass mixing at this innermost station was

197   not as straightforward, despite minor freshwater admixture as suggested by the high surface

198   salinity of >32.0.

199   The TAlk-Sal relationship in the upper 175 m waters on Transects 5 and 6 displayed two

200   similar phases. One was the linear regression for stations 35-38 (deeper than ~800 m) and

201   stations 45-49 (deeper than ~1400 m), with slope and intercept values comparable to the second

202   phase observed on Transect 4. The other was the linear regression for the three shallow stations

203   on both transects largely influenced by coastal upwelling (Feely et al., 2008) (Fig. 3b and 3c).

204   This phase was not clearly seen from the full TAlk-Sal plot (Fig. 2b and 2c), as the salinity in the

205   upper 175 m waters at stations 39 and 44 as well as in the entire water column of stations 40-43

206   varied within a much smaller range of ~33.3-~34.0. The negligible intercepts of this TAlk-Sal

207   regression suggested insignificant freshwater input with zero solutes to the intensive upwelling

208   zone off Oregon and northern California (Fig. 3b and 3c).

209   All phases shown in Fig. 3 displayed good linear TAlk-Sal relationships (r>0.94), indicating

210   an overall two end-member mixing scheme for each phase. Although the non-conservativity of

211　TAlk existed, it was not that significant as seen by the deviations of a few data points from each

212　linear regression (Fig. 3). As a matter of fact, Fassbender et al. (2011) estimate that the

213　contribution from $CaCO_3$ dissolution to the TAlk addition in the surface mixed layer on Transect

214　5 was <10 μmol kg^{-1} (<0.5% of their absolute contents in seawater) and well around the

215　analytical precision. Such small non-conservative portions would not compromise the

216　application of TAlk as a conservative tracer. Note that the two end-member mixing was not

217　spatially homogeneous in the upper waters off Oregon and northern California during the

218　sampling period. The top waters at stations 26-32 on Transect 4 were imprinted by the CR plume

219　with a salinity around ~30.0. During the transport from the mouth of the CR estuary, the plume

220　water increasingly mixed with adjacent oceanic waters, largely feeding its pathway. However,

221　the majority of DIC and nutrients in waters immediately below the buoyant layer, as well as in

222　surface waters at station 33 and possibly at station 25, originated from deep waters through

223　coastal upwelling and/or vertical mixing. The influence of the CR plume still occurred but was

224　diluted by other freshwater masses such as rainwater, suggesting a mixing scheme between the

225　deep water in the subtropical gyre of the eNP and a combined freshwater end-member (Park,

226　1966, 1968). Such mixing was also applicable to the surface waters at stations 35-38 on Transect

227　5 and stations 45-49 on Transect 6. On the other hand, the upper 175 m waters or the entire water

228　column at stations 39-44 resulted from a simple two end-member mixing between the upwelling

229　source water and the rainwater with zero solutes, establishing for them an apparent OceMar-type

230　system.

231　**3.2 ΔDIC and ΔNO$_3$ in the upper waters off Oregon and northern California**

11

232   The defined mixing schemes enabled us to estimate the non-conservative portion of DIC

233   (ΔDIC) and NO$_3$ (ΔNO$_3$) in the upper waters off Oregon and northern California following Dai

234   et al. (2013):

235    $\Delta DIC = DIC^{cons} - DIC^{meas}$ (1)

236    $\Delta NO_3 = NO_3^{cons} - NO_3^{meas}$ (2)

237    $X^{cons} = \dfrac{Sal^{meas}}{Sal^{ref}} \times (X^{ref} - X^{eff}) + X^{eff}$ (3)

238   The superscripts "cons" and "meas" in Eqs (1) and (2) denote conservative-mixing induced and

239   field measured values. In Eq. (3), X represents DIC or NO$_3$ while Sal^{meas} is the CTD measured

240   salinity. Sal^{ref} and X^{ref} are the reference salinity and concentration of DIC or NO$_3$ for the deep

241   water end-member, which are the averages of all ~175 m samples from stations involved in each

242   mixing scheme. Specifically, for waters immediately below the top buoyant layer at stations 27-

243   32 and waters in the surface mixed layer at stations 25 and 33 on Transect 4, the deep water end-

244   member values of the reference salinity and concentrations of DIC or NO$_3$ were the averages of

245   ~175 m samples from stations 28-33 (Fig. 1). On Transects 5 and 6, the preformed salinity, DIC

246   and NO$_3$ values for waters in the surface mixed layer at stations 35-38 and at stations 45-49 were

247   the averages of ~175 m samples of these stations. For the upper waters influenced by the

248   intensified upwelling at stations 39-41 and stations 42-44, the deep water end-member was

249   selected as the ~175 m water at station 39 and at station 44 (Fig. 1).

250   The X^{eff} in Eq. (3) denotes the effective concentration of DIC or NO$_3$ sourced from the

251   freshwater input to various zones off Oregon and northern California. Since rainwater was

252   assumed to have no solutes, both DIC^{eff} and NO$_3$^{eff} would be zero for waters in the surface mixed

253   layer of stations 39-41 on Transect 5 and stations 42-44 on Transect 6. On the other hand, the

254 estimation of X^{eff} associated with the CR followed the method for the OceMar case study of the

255 CS, which has a noticeable DIC^{eff} from the combination of the Amazon River and the Orinoco

256 River (Dai et al., 2013).

257 Since bicarbonate dominates other CO_2 species and other alkalinity components, DIC

258 concentrations in the main stream of the CR are numerically similar to TAlk, which are also

259 around ~1000 µmol kg^{-1} (Park et al., 1969a, 1970). This value was taken as the DIC end-member

260 of the CR. The NO_3 end-member value was selected as 15 µmol kg^{-1} based on recent years'

261 observations in May and June at station SATURN-05 established in the upstream CR (database

262 of the Center for Coastal Margin Observation and Prediction;

263 http://www.stccmop.org/datamart/observation_network/fixedstation?id=saturn05#anchor_5).

264 Assuming that the biological consumption of DIC and NO_3 in the CR plume followed the

265 Redfield ratio (Redfield et al., 1963), the DIC removal was estimated to be ~100 µmol kg^{-1}

266 (approximately 15·106/16), while NO_3 was rapidly consumed along the pathway of the CR

267 plume and generally depleted in the area beyond the plume (Aguilar-Islas and Bruland, 2006;

268 Lohan and Bruland, 2006). As a consequence, the complete DIC^{eff} and NO_3^{eff} in the upper waters

269 from the CR would be ~900 µmol kg^{-1} and ~0 µmol kg^{-1}.

270 If the combined freshwater end-member was a mixture of the CR and the rainwater with zero

271 solutes, the intercept values of 521.0±30.6 (Fig. 3a), 677.4±32.2 (Fig. 3b) and 609.9±34.1 (Fig.

272 3c) derived from the TAlk-Sal regression indicated that the CR fractions were ~50, ~65 and ~60%

273 (approximately 500/1000, 650/1000 and 600/1000 taking ~1000 µmol kg^{-1} as the TAlk end-

274 member value of the CR, Park et al., 1969b; Evans et al., 2013). The DIC^{eff} from the freshwater

275 input was thus estimated to be ~450 µmol kg^{-1} (approximately 900·50%) for waters immediately

276 below the top buoyant layer at stations 27-32 and waters in the surface mixed layer at stations 25

13

277 and 33 on Transect 4, which was slightly lower than the ~585 μmol kg^{-1} (approximately

278 900·65%) and the ~540 μmol kg^{-1} (approximately 900·60%) for waters in the surface mixed

279 layer at stations 35-38 on Transect 5 and at stations 45-49 on Transect 6, respectively. The NO_3^{eff}

280 in any combined freshwater end-member was zero.

281   Note that numerous small mountainous rivers are distributed on the Oregon-California coast,

282 which might also have diluted the CR plume inducing the lower intercept of the TAlk-Sal

283 regression observed on the three transects (Fig. 3). The average wintertime discharge from these

284 Coast Range rivers is estimated to be ~2570 m^3 s^{-1} (Wetz et al., 2006), which is more than an

285 order of magnitude higher than that in the summer (Colbert and McManus, 2003; Sigleo and

286 Frick, 2003). However, the CR discharge in May to June 2007 reached its maximum of ~15000

287 m^3 s^{-1} (Evans et al., 2013), which should be approximately two orders of magnitude higher than

288 the discharge of small rivers. This significant contrast would suggest that inputs from small

289 rivers should be negligible compared to the CR plume. In particular, inputs from small rivers are

290 normally restricted to a narrow band near the coast, whereas the research domain of this study

291 extended to the open subtropical gyre of the eNP. Even the surface salinity at the innermost

292 stations (i.e., station 25 on Transect 4, station 41 on Transect 5 and station 42 on Transect 6; Fig.

293 1) was as high as ~32.5, ~33.9 and ~34.0, which would rule out the influence of small rivers.

294 **3.3 Evaluating the CO$_2$ source/sink nature in the upper waters off Oregon and northern**

295 **California**

296   The coupling of DIC and NO$_3$ dynamics could then be examined based on the classic Redfield

297 ratio of C:N=106:16=6.6 (Redfield et al., 1963). Positive values of the difference between ΔDIC

298 and 6.6ΔNO$_3$ (ΔDIC−6.6ΔNO$_3$) suggested a CO$_2$ source term since "excess ΔDIC" was removed

299 by CO$_2$ degassing into the atmosphere. In contrast, negative ΔDIC−6.6ΔNO$_3$ suggested that

14

300 "deficient ΔDIC" was supplied via the atmospheric CO_2 input to the ocean representing a CO_2

301 sink. Such net CO_2 exchange between the seawater and the atmosphere was further quantified as

302 the sea-air difference of pCO_2 (ΔpCO_2) via the Revelle factor (RF), which is referred to as the

303 fractional change in seawater CO_2 over that of DIC at a given temperature, salinity and alkalinity

304 and indicates the ocean's sensitivity to an increase in atmospheric CO_2 (Revelle and Suess, 1957;

305 Sundquist et al., 1979). Because pCO_2 and CO_2 are proportional to each other, the RF can be

306 illustrated as:

307 $$RF = \frac{\partial pCO_2 / pCO_2}{\partial DIC / DIC} \quad (4)$$

308 Here, ∂pCO_2 and ∂DIC are the fractional changes of pCO_2 and DIC in the surface seawater. In

309 the OceMar framework, ∂DIC equals $\Delta DIC - 6.6\Delta NO_3$ that is solely achieved through air-sea

310 CO_2 exchange, implying that ∂pCO_2 represents the sea-air ΔpCO_2. Given an initial balance of

311 CO_2 between the seawater and the atmosphere, the sea-air ΔpCO_2 is obtained by:

312 $$Sea\text{-}air\,\Delta pCO_2 = \partial pCO_2 = RF \times pCO_2 \times \frac{\partial DIC}{DIC} = RF \times pCO_2^{air} \times \frac{\Delta DIC - 6.6\Delta NO_3}{DIC} \quad (5)$$

313 As shown in Fig. 4, the estimated $\Delta DIC - 6.6\Delta NO_3$ values and their corresponding sea-air

314 ΔpCO_2 in the upper waters off Oregon and northern California were overall below zero,

315 suggesting a significant CO_2 sink nature in the upwelling season.

316 **3.3.1 Transect 4**

317 On Transect 4 off Newport, the average value of $\Delta DIC - 6.6\Delta NO_3$ was -23 ± 2 μmol kg^{-1} in

318 waters immediately below the top buoyant layer at stations 27-32, which equaled the average

319 value for the surface mixed layer at station 33 (Fig. 4a). Note that we were not able to derive

320 values of $\Delta DIC - 6.6\Delta NO_3$ at station 26 where NO_3 data were not available. Although located at

321 different depths, the two water parcels experienced similar physical mixing and biogeochemical

322   modifications inducing the same CO_2 signature. The former water mass should work as a CO_2

323   sink when in contact with the atmosphere before or after the passage of the episodic CR plume.

324   The average sea-air ΔpCO_2 resulting from the combined deficient ΔDIC was -54 ± 4 μatm (Fig.

325   3a). Given the atmospheric pCO_2 of ~390 μatm (Evans et al., 2011), the seawater pCO_2 in these

326   regions was thus estimated to be 336 ± 4 μatm, which agreed rather well with the field

327   measurements of 334 ± 13 μatm (the underway seawater pCO_2 data were not available online but

328   alternatively calculated by applying TAlk and DIC data into the CO2SYS program, Lewis and

329   Wallace, 1998).

330   The diagnostic approach was not applied to the top buoyant layer since the aged CR plume

331   might have experienced complex mixing with various surrounding water masses during its

332   transport, as indicated by the scatter TAlk-Sal relationship (Fig. 3a). However, the far-field CR

333   plume is suggested to be a strong sink of atmospheric CO_2 due to earlier biological consumption

334   (Evans et al., 2011), which was supported by the observed low pCO_2 of ~220-300 μatm in the

335   top buoyant layer on Transect 4. As a consequence, the CO_2 sink nature in the upper waters from

336   the outer shelf (the bottom depth of station 27 was ~170 m) to the open basin off Newport,

337   Oregon would primarily result from the higher utilization of nutrients relative to DIC based on

338   their concurrent inputs from deep waters. The non-local high productivity in the CR plume could

339   inject even lower pCO_2 but this effect would be transitory.

340   At the innermost station 25 on Transect 4, highly positive values of $\Delta DIC-6.6\Delta NO_3$ and sea-

341   air ΔpCO_2 (~82 μmol kg^{-1} and ~157 μatm, respectively) were obtained for the surface mixed

342   layer of this station, indicating a significant CO_2 source. However, the lowest pCO_2 value of

343   ~170 μatm was observed in these nearshore waters off Oregon. The poor correlation between

344   TAlk and salinity at station 25 (Fig. 3a) might compromise the estimation, whereas the same

345 method (Eqs 1-5) was successfully applied to other stations on Transect 4 with a distinct TAlk-

346 Sal relationship (i.e., the second phase in Fig. 3a). Note that coastal upwelling clearly influenced

347 the bottom water at station 25 as indicated by the comparable salinity and TAlk values to those in

348 offshore 200 m waters. Instead of being fed by the upwelled deep water, the DIC and nutrients in

349 the surface mixed layer might have originated from horizontal admixture of the surrounding

350 waters. These waters possibly experienced intense diatom blooms due to the fact that the surface

351 silicate concentrations at station 25 were almost zero, which led to the most undersaturated pCO_2

352 condition observed in the upper waters off Oregon.

353 **3.3.2 Transects 5 and 6**

354 On Transect 5 near the Oregon-California border, the average $\Delta DIC−6.6\Delta NO_3$ and sea-air

355 ΔpCO_2 were estimated to be $−20\pm3$ μmol kg^{-1} and $−48\pm8$ μatm in the surface mixed layer of

356 stations 35-38 (Fig. 4b). Both values were comparable to those obtained from the surface mixed

357 layer of stations 45-49 on Transect 6 ($−23\pm3$ μmol kg^{-1} and $−53\pm6$ μatm, respectively; Fig. 4c)

358 and on Transect 4, indicating a similar magnitude of the CO_2 sink term in offshore areas along

359 the Oregon and northern California coast during the sampling period. The estimated sea surface

360 pCO_2 of 342 ± 8 μatm for Transect 5 and 337 ± 6 μatm for Transect 6 were consistent with the field

361 measurements of 332 ± 12 and 346 ± 12 μatm in these regions.

362 The diagnosed CO_2 flux in the nearshore was also comparable between Transects 5 and 6. The

363 $\Delta DIC−6.6\Delta NO_3$ and sea-air ΔpCO_2 in the surface mixed layer of stations 39-44, although still

364 below zero, were obviously higher than those of stations 35-38 on Transect 5 and of stations 45-

365 49 on Transect 6 (Fig. 4b and 4c). Such an increase was expected since stations 39-44 were

366 located in the area with the most intensive upwelling, which brought CO_2-rich deep waters to the

367 nearshore surface (Feely et al., 2008). However, our estimation suggested a weaker CO_2 sink or

368 close to being in equilibrium with the combined estimated sea surface pCO_2 of 368±14 µatm,

369 whereas the field measurements of ~600-1000 µatm indicated that the coastal upwelling zone

370 should be a very strong source of CO_2 to the atmosphere.

371 Therefore, we took a closer look at Transect 5: A uniform salinity of ~34.0 through the entire

372 water column was observed at stations 40 and 41 due to the outcrop of the upwelling source

373 water at the surface of the inner shelf on Transect 5 (Feely et al., 2008). Although salinity in the

374 surface mixed layer at station 39 was lower, around ~33.4, the dilution effect of rainwater should

375 be negligible. After removing the rainwater from the mixing scheme and calculating ΔDIC and

376 ΔNO_3 by directly subtracting the field observed value from the end-member value for the

377 upwelling source water (Eqs 6 and 7; DIC^{ref} and NO_3^{ref} were field measurements of ~200 m

378 water samples at station 39), the $\Delta DIC−6.6\Delta NO_3$ values were rapidly increased to above zero in

379 the surface mixed layer at stations 39 and 40, while values at station 41 with a small increase

380 were still overall below zero (Fig. 5a). Correspondingly, the estimated sea surface pCO_2 values

381 were higher than the atmospheric CO_2 value at stations 39 and 40 while they were slightly lower

382 than that at station 41. However, these values still largely fell below the field measurements of

383 seawater pCO_2, displaying shoreward increasing differences from ~200 to ~700 µatm (Fig. 5b).

384 $$\Delta DIC = DIC^{ref} - DIC^{meas} \quad (6)$$

385 $$\Delta NO_3 = NO_3^{ref} - NO_3^{meas} \quad (7)$$

386 With or without taking rainwater into account, our diagnostic approach did not work in the

387 nearshore with strong upwelling off Oregon and northern California, even though the mixing

388 scheme of this region was in accordance with the OceMar concept. We contend that OceMar

389 assumes a steady state with balanced DIC and nutrients via both physical mixing and biological

390 alterations in comparable timescales. However, the continuous inputs from the coastal upwelling

391   might have led to the accumulation of DIC and nutrients in the nearshore surface, which could

392   not be timely consumed by the phytoplankton community, suggesting a possible non-steady

393   state. Fassbender et al. (2011) estimate that the age of the surface mixed layer at nearshore

394   stations on Transect 5 is only ~0.2 days, during which the DIC and NO_3 consumption via organic

395   carbon production was almost zero and $CaCO_3$ dissolution contributed a small fraction to the

396   slightly elevated DIC in the upwelled waters. They further predict that the nearshore surface

397   pCO_2 on Transect 5 will decrease to levels of ~200 µatm in ~30 days until NO_3 exhaustion via

398   continued biological productivity, implying the achievement of a steady state (Fassbender et al.,

399   2011). Minor biological responses during the intensified upwelling period were also observed in

400   summer 2008, allowing highly oversaturated pCO_2 surface water to persist on the inner shelf off

401   Oregon for nearly two months (Evans et al., 2011). At this point, it is uncertain why there was

402   such a prolonged delay from the phytoplankton community to the persistent source of upwelled

403   DIC and nutrients. Note that under the condition of a more prevailing upwelling-favorable wind

404   as a predicted consequence of climate change (e.g., Snyder et al., 2003; Diffenbaugh et al., 2004;

405   Sydeman et al., 2014), the nearshore waters off the Oregon-California coast in the upwelling

406   season might always be in a non-steady state, and it is expected that fewer periodic relaxation

407   events or reversals would further decrease the chance for the biological response to be factored

408   in.

409   In addition, the negligible biological consumption might involve large errors when calculating

410   Δ. The portion of ΔDIC and $ΔNO_3$ at station 41 relative to the preformed values of the upwelling

411   source water were only ~0.5 and ~10%, slightly higher than the measurement uncertainties. The

412   portion of DIC and NO_3 consumption in the surface mixed layer at offshore stations on Transect

413   5 were, however, one order of magnitude higher (~7 and ~90%, respectively). This contrast

414   might partially explain why the OceMar framework did not work when insignificant biological

415   alterations occurred. Given the predominant control of physical mixing, we contend that the

416   prediction of the CO_2 flux in the nearshore off Oregon and northern California with intensified

417   upwelling could be simplified without considering DIC/nutrient consumption. In other words,

418   surface CO_2 levels in this region were simply imprints of the upwelling source water (pCO_2

419   ~1000 μatm at ~150-200 m) with minor dilution by rainwater.

420   **3.4 Sensitivity analysis**

421   In the above exercise, both the end-member values revealed in the water mass mixing scheme

422   and the Redfield ratio adopted in coupling DIC and nutrients were critically important in

423   resolving the CO_2 fluxes. We thus conducted sensitivity analysis for these two sets of variables

424   for the CO_2 sink zones off Oregon and northern California where our diagnostic approach

425   worked well (i.e., waters immediately below the top buoyant layer at stations 27-32 as well as

426   waters in the surface mixed layer at station 33 on Transect 4, waters in the surface mixed layer at

427   stations 35-38 on Transect 5 and waters in the surface mixed layer at stations 45-49 on Transect

428   6).

429   **3.4.1 The combined freshwater end-member**

430   While the values of ~1000 and ~15 μmol kg^{-1} were selected for TAlk/DIC and NO_3 in the

431   main stream of the CR, the field observed TAlk and NO_3 varies within a range of ~800-1200

432   (Evans   et   al.,   2013)   and   ~10-20   μmol   kg^{-1}

433   (http://www.stccmop.org/datamart/observation_network/fixedstation?id=saturn05#anchor_5)   in

434   spring/early summer. We thus took the values of ~800 and ~1200 μmol kg^{-1} as the lower and

435   upper limit of the TAlk and DIC end-members, and those of ~10 and ~20 μmol kg^{-1} as the lower

436   and upper limit of the NO_3 end-member in the CR to test the diagnostic approach. Following the

437   same calculation of the combined freshwater end-member (X^{eff} in Eq. 3), the lower and upper

438   limit of DIC^{eff} was estimated to be ~420 and ~470 $\mu mol \ kg^{-1}$, for waters immediately below the

439   top buoyant layer at stations 27-32 and in the surface mixed layer at station 33 on Transect 4.

440   Those values were ~540 and ~610 $\mu mol \ kg^{-1}$ for waters in the surface mixed layer at stations 35-

441   38 on Transect 5, and ~500 and ~570 $\mu mol \ kg^{-1}$ in the surface mixed layer at stations 45-49 on

442   Transect 6. The NO_3^{eff} in any scenario was still zero.

443   The newly diagnosed $\Delta DIC - 6.6\Delta NO_3$ and sea-air ΔpCO_2 on Transects 4, 5 and 6 displayed no

444   difference with those with the initial TAlk and DIC of ~1000 $\mu mol \ kg^{-1}$ and NO_3 of ~15 $\mu mol \ kg^{-}$

445   ^{1} in the CR (Table 1), while all estimated sea surface pCO_2 values were within error compared to

446   the field measurements. Although the TAlk and DIC end-members had large variations of up to

447   ~400 $\mu mol \ kg^{-1}$ while NO_3 varied within ~10 $\mu mol \ kg^{-1}$ in the main stream of the CR, the

448   corresponding range of DIC^{eff} contributing to waters beyond the CR plume significantly

449   decreased by approximately one order of magnitude, implying minor influence of its variations

450   on our diagnosis of the CO_2 fluxes.

451   **3.4.2 The deep water end-member**

452   We selected values at ~175 m as the deep water end-member based on the TAlk-Sal

453   relationship, whereas this end-member depth might not be spatially stable in a highly dynamic

454   upwelling system. Previous studies also show that the upwelling source water onto the Oregon-

455   California shelf can vary between 150 and 200 m (e.g., Hales et al., 2005; Feely et al., 2008). We

456   thus tested the diagnostic approach with values at three other depths of ~130, ~150 and ~200 m.

457   On Transects 4 and 6, the newly estimated $\Delta DIC - 6.6\Delta NO_3$, sea-air ΔpCO_2 and sea surface

458   pCO_2 using end-member values at both ~150 and ~200 m agreed well with those using end-

459   member values at ~175 m, while the three variables were slightly higher using end-member

460 values at ~130 m (Table 2). On Transect 5, the newly estimated $\Delta DIC-6.6\Delta NO_3$, sea-air ΔpCO_2

461 and sea surface pCO_2 using end-member values at both ~130 and ~150 m agreed well with those

462 using end-member values at ~175 m, while the three variables were slightly higher using end-

463 member values at ~200 m (Table 2).

464 3.4.3 The C/N uptake ratio

465   In a given oceanic setting, the real C/N uptake ratio during organic carbon production can be

466 different from the Redfield stoichiometry of ~6.6 (Redfield et al., 1963). For instance, higher

467 ratios estimated from the DIC-NO_3 relationship are observed in both coastal waters and open

468 ocean sites, possibly resulting from excess DIC uptake via the production of dissolved organic

469 carbon (Sambrotto et al., 1993; Ianson et al., 2003). However, since the precise estimation of the

470 C/N uptake ratio (via e.g. in situ incubation experiments) is still problematic, such data are

471 currently scarce over the world's oceans and the empirical stoichiometry is routinely applied into

472 field studies investigating the dynamics and coupling of carbon and nutrients (e.g., Chen et al.,

473 2008; Fassbender et al., 2011). Fassbender et al. (2011) apply another empirical C/N uptake ratio

474 of 7.3 (approximately 117/16; Anderson and Sarmiento, 1994) into the same data set as this

475 study. We thus performed a simple sensitivity analysis using this alternative value of 7.3, which

476 implies excess DIC uptake relative to NO_3.

477   Since $\Delta DIC-7.3\Delta NO_3$ values were obviously smaller than $\Delta DIC-6.6\Delta NO_3$ ones, the new sea-

478 air ΔpCO_2 values were halved (Table 3). Correspondingly, the newly estimated sea surface pCO_2

479 values on Transects 4, 5 and 6 were ~35-45 µatm lower than the estimation using the Redfield

480 ratio, which were however consistent with the field measurements. Given that the Redfield ratio

481 also works in our OceMar case studies of the SCS and the CS (Dai et al., 2013), we contend that

482 this classic ratio could be preferentially employed if the field observed elemental stoichiometry

22

483   is not available. Moreover, as Martz et al. (2014) point out, "treating the Redfield ratios as global

484   or regional constants may be acceptable in the context of interpreting snapshots of the water

485   column captured in shipboard bottle data".

486   The above notion was also supported by examining the slope of the linear regression between

487   DIC and NO_3 normalized to a constant salinity in the surface water or in the surface mixed layer,

488   which provides an alternative to the C/N uptake ratio associated with organic carbon production

489   (Sambrotto et al., 1993; Wong et al., 2002; Ianson et al., 2003). Given a non-zero combined

490   freshwater end-member, we adopted in this study an approach of regional normalization (Friis et

491   al., 2003; Cao et al., 2011) as:

492   $$nX = \frac{X^{meas} - X^{eff}}{Sal^{meas}} \times Sal^{aver} + X^{eff} \quad (8)$$

493   Here, nX and X^{meas} are salinity normalized and field measured values for DIC and NO_3. Sal^{meas} is

494   the CTD measured salinity. Sal^{aver} is the average salinity value of ~33.0 in these CO_2 sink zones,

495   which was selected as the constant salinity. X^{eff} is the same as that in Eq. (3), denoting the

496   effective concentration of DIC or NO_3 sourced from the freshwater input to various zones off

497   Oregon and northern California. While the NO_3^{eff} in any combined freshwater end-member was

498   zero, the DIC^{eff} was ~450 μmol kg^{-1} for waters immediately below the top buoyant layer at

499   stations 27-32 and waters in the surface mixed layer at stations 25 and 33 on Transect 4, ~585

500   μmol kg^{-1} for waters in the surface mixed layer at stations 35-38 on Transect 5, and ~540 μmol

501   kg^{-1} for waters in the surface mixed layer at stations 45-49 on Transect 6.

502   As shown in Fig. 6, our analysis with all data from the CO_2 sink zones along the three

503   transects revealed a slope of 6.70±0.37. This value was within error comparable to that of 6.6,

504   suggesting that using the Redfield ratio in our diagnostic approach should be in order. On the

505   other hand, we contend that scrutinizing the in situ C/N uptake ratio via relatively direct

506 observations is imperative, for better understanding the issue regarding the possible departure

507 from the Redfield ratio.

4 Concluding remarks

509 The semi-analytical diagnostic approach of mass balance that couples physical transport and

510 biogeochemical alterations was well applied to the CO_2 sink zones off Oregon and northern

511 California in spring/early summer 2007, extending from the outer shelf to the open basin. In

512 these zones with the absence of any significant influence of the CR plume, the source of DIC

513 was largely from deep waters in the subtropical gyre of the eNP and the ultimate CO_2 sink nature

514 was determined by the higher nutrient consumption than DIC in the upper waters. On the other

515 hand, the estimated CO_2 flux was opposite to the field observations in the coastal upwelling zone

516 along the Oregon-California coast, which behaved like a typical OceMar system in terms of its

517 mixing process. This discrepancy was very likely due to minor biological responses during the

518 intensified upwelling period, making our mass balance approach based on the coupled physical

519 biogeochemistry invalid. This suggested that the applicability of the proposed semi-analytical

520 diagnostic approach is limited to steady state systems with comparable timescales of water mass

521 mixing and biogeochemical reactions. In such a physical mixing prevailing regime, resolving the

522 CO_2 fluxes could be simplified without considering the biological consumption of DIC and

523 nutrients. Further work is however needed to understand the carbon and nutrient dynamics as

524 well as the timing between physics and biology associated with coastal upwelling.

References

Aguilar-Islas, A. M., and Bruland, K. W.: Dissolved manganese and silicic acid in the Columbia River plume: A major source to the California current and coastal waters off Washington and Oregon, Mar. Chem., 101, 233-247, 2006.

Allen, J. S., Newberger, P. A., and Federiuk, J.: Upwelling circulation on the Oregon continental shelf. Part I: Response to idealized forcing, J. Phys. Oceanogr., 25, 1843-1866, 1995.

Anderson, L. A., and Sarmiento, J. L.: Redfield ratios of remineralization determined by nutrient data analysis, Global Biogeochem. Cycles, 8, 65-80, 1994.

Barth, J. A. and Smith, R. L.: Separation of a coastal upwelling jet at Cape Blanco, Oregon, USA, in: Benguela Dynamics: Impacts of Variability on Shelf-Sea Environments and their Living Resources, edited by S. C. Pillar, C. L. Moloney, A. I. L. Payne, and F. A. Shillington, S. Afr. J. Mar. Sci., 19, 5-14, 1998.

Barth, J. A., Pierce, S. D., and Smith, R. L.: A separating coastal upwelling jet at Cape Blanco, Oregon and its connection to the California Current System, Deep-Sea Res. II, 47, 783-810, 2000.

Borges, A. V.: Present day carbon dioxide fluxes in the coastal ocean and possible feedbacks under global change, in: Oceans and the Atmospheric Carbon Content, edited by P. Duarte, and J. M. Santana-Casiano, Springer Science+Business Media B.V., chap. 3, 47-77, 2011.

Borges, A. V., Delille, B., and Frankignoulle, M.: Budgeting sinks and sources of CO_2 in the coastal ocean: Diversity of ecosystems counts, Geophys. Res. Lett., 32, L14601, doi:10.1029/2005GL023053, 2005.

Borges, A. V., and Frankignoulle, M.: Distribution of surface carbon dioxide and air-sea exchange in the upwelling system off the Galician coast, Global Biogeochem. Cycles, 16,

558   1020, doi:10.1029/2000GB001385, 2002.

559   Cai, W.-J.: Estuarine and coastal ocean carbon paradox: CO_2 sinks or sites of terrestrial carbon

560   incineration?, Annu. Rev. Mar. Sci., 3, 123-145, 2011.

561   Cai, W.-J., Dai, M., and Wang, Y.: Air-sea exchange of carbon dioxide in ocean margins: A

562   province-based synthesis, Geophys. Res. Lett., 33, L12603, doi:10.1029/2006GL026219,

563   2006.

564   Cao, Z., Dai, M., Zheng, N., Wang, D., Li, Q., Zhai, W., Meng, F., and Gan, J.: Dynamics of the

565   carbonate system in a large continental shelf system under the influence of both a river

566   plume and coastal upwelling, J. Geophys. Res., 116, G02010, doi:10.1029/2010JG001596,

567   2011.

568   Castro, C. G., Chavez, F. P., and Collins, C. A.: Role of the California Undercurrent in the export

569   of denitrified waters from the eastern tropical North Pacific, Global Biogeochem. Cycles,

570   15(4), 819-830, doi:10.1029/2000GB001324, 2001.

571   Chase, Z., Strutton, P. G., and Hales, B.: Iron links river runoff and shelf width to phytoplankton

572   biomass along the U.S. West Coast, Geophys. Res. Lett., 34, L04607,

573   doi:10.1029/2006GL028069, 2007.

574   Chen, C.-T. A., and Borges, A. V.: Reconciling opposing views on carbon cycling in the coastal

575   ocean: Continental shelves as sinks and near-shore ecosystems as sources of atmospheric

576   CO_2, Deep-Sea Res. II, 56, 578-590, 2009.

577   Chen, F., Cai, W.-J., Wang, Y., Rii, Y. M., Bidigare, R. R., and Benitez-Nelson, C. R.: The carbon

578   dioxide system and net community production within a cyclonic eddy in the lee of Hawaii,

579   Deep-Sea Res. II, 55, 1412-1425, 2008.

580   Colbert, D., and McManus, J.: Nutrient biogeochemistry in an upwelling-influenced estuary of

581   the Pacific Northwest (Tillamook Bay, Oregon, USA), Estuaries, 26, 1205-1219, 2003.

582 Dai, M., Cao, Z., Guo, X., Zhai, W., Liu, Z., Yin, Z., Xu, Y., Gan, J., Hu, J., and Du, C.: Why are

583   some marginal seas sources of atmospheric CO_2?, Geophys. Res. Lett., 40, 2154-2158,

584   doi:10.1002/grl.50390, 2013.

585 Diffenbaugh, N. S., Snyder, M. A., and Sloan, L. C.: Could CO_2-induced land-cover feedbacks

586   alter near-shore upwelling regimes?, Proc. Natl. Acad. Sci. USA, 101, 27-32, 2004.

587 Evans, W., Hales, B., and Strutton, P. G.: Seasonal cycle of surface ocean pCO$_2$ on the Oregon

588   shelf, J. Geophys. Res., 116, C05012, doi:10.1029/2010JC006625, 2011.

589 Evans, W., Hales, B., and Strutton, P. G.: pCO$_2$ distributions and air-water CO_2 fluxes in the

590   Columbia River estuary, Estuar. Coast. Shelf Sci., 117, 260-272, 2013.

591 Evans, W., Hales, B., Strutton, P. G., and Ianson, D.: Sea-air CO_2 fluxes in the western Canadian

592   coastal ocean, Prog. Oceanogr., 101, 78-91, 2012.

593 Fassbender, A. J., Sabine, C. L., Feely, R. A., Langdon, C., and Mordy, C. W.: Inorganic carbon

594   dynamics during northern California coastal upwelling, Cont. Shelf Res., 31, 1180-1192,

595   2011.

596 Federiuk, J., and Allen, J. S.: Upwelling circulation on the Oregon continental shelf. Part II:

597   Simulations and comparisons with observations, J. Phys. Oceanogr., 25, 1867-1889, 1995.

598 Feely, R., and Sabine, C.: Carbon dioxide and hydrographic measurements during the 2007

599   NACP   West   Coast   Cruise,

600   http://cdiac.ornl.gov/ftp/oceans/NACP_West_Coast_Cruise_2007/,   Carbon   Dioxide

601   Information Analysis Center, Oak Ridge National Laboratory, US Department of Energy,

602   Oak   Ridge,   Tennessee,   doi:

603   10.3334/CDIAC/otg.CLIVAR_NACP_West_Coast_Cruise_2007, 2011.

604 Feely, R. A., Sabine, C. L., Hernandez-Ayon, J. M., Ianson, D., and Hales, B.: Evidence for

605   upwelling of corrosive "acidified" water onto the continental shelf, Science, 320, 1490-1492,

606   2008.

607 Fransson, A., Chierici, M., and Nojiri, Y.: Increased net CO_2 outgassing in the upwelling region

608   of the southern Bering Sea in a period of variable marine climate between 1995 and 2001, J.

609   Geophys. Res., 111, C08008, doi:10.1029/2004JC002759, 2006.

610 Friederich, G. E., Walz, P. M., Burczynski, M. G., and Chavez, F. P.: Inorganic carbon in the

611   central California upwelling system during the 1997-1999 El Niño-La Niña event, Prog.

612   Oceanogr., 54, 185-203, 2002.

613 Friis, K., Körtzinger, A., and Wallace, D. W. R.: The salinity normalization of marine inorganic

614   carbon chemistry data, Geophys. Res. Lett., 30(2), 1085, doi:10.1029/2002GL015898, 2003.

615 Gan, J. and Allen, J. S.: A modeling study of shelf circulation off northern California in the

616   region of the Coastal Ocean Dynamics Experiment, response to relaxation of upwelling, J.

617   Geophys. Res., 107(C9), 3123, doi:10.1029/2000JC000768, 2002.

618 Gan, J., and Allen, J. S.: Modeling upwelling circulation off the Oregon coast, J. Geophys. Res.,

619   110, C10S07, doi:10.1029/2004JC002692, 2005.

620 Hales, B., Takahashi, T., and Bandstra, L.: Atmospheric CO_2 uptake by a coastal upwelling

621   system, Global Biogeochem. Cycles, 19, GB1009, doi:10.1029/2004GB002295, 2005.

622 Hales, B., Struttong, P. G., Saraceno, M., Letelier, R., Takahashi, T., Feely, R., Sabine, C., and

623   Chavez, F.: Satellite-based prediction of pCO_2 in coastal waters of the eastern North Pacific,

624   Prog. Oceanogr., 103, 1-15, 2012.

625 Hickey, B. M.: Patterns and processes of circulation over the Washington continental shelf and

626   slope, in: Coastal Oceanography of Washington and Oregon, Elsevier Sci., New York, 41-

627   115, doi:10.1016/S0422-9894(08)70346-5, 1989.

628   Hill, J. K., and Wheeler, P. A.: Organic carbon and nitrogen in the northern California current

629   system: comparison of offshore, river plume, and coastally upwelled waters, Prog.

630   Oceanogr., 53, 369-387, 2002.

631   Huyer, A.: Coastal upwelling in the California Current system, Prog. Oceanogr., 12, 259-284,

632   1983.

633   Ianson, D., Allen, S. E., Harris, S. L., Orians, K. J., Varela, D. E., and Wong, C. S.:The inorganic

634   carbon system in the coastal upwelling region west of Vancouver Island, Canada, Deep-Sea

635   Res. I, 50, 1023-1042, 2003.

636   Kosro, P. M., Huyer, A., Ramp, S. R., Smith, R. L., Chavez, F. P., Cowles, T. J., Abbott, M. R.,

637   Strub, P. T., Barber, R. T., Jessen, P., and Small, L. F.: The structure of the transition zone

638   between coastal waters and the open ocean off northern California, winter and spring 1987,

639   J. Geophys. Res., 96(8), 14707-14730, 1991.

640   Laruelle, G. G., Dürr, H. H., Slomp, C. P., and Borges, A. V.: Evaluation of sinks and sources of

641   CO_2 in the global coastal ocean using a spatially-explicit typology of estuaries and

642   continental shelves, Geophys. Res. Lett., 37, L15607, doi:10.1029/2010GL043691, 2010.

643   Lewis, E., and Wallace, D. W. R.: Program Developed for CO_2 System Calculations,

644   ORNL/CDIAC-105, Carbon Dioxide Information Analysis Center, Oak Ridge National

645   Laboratory, U.S. Department of Energy, Oak Ridge, TN, 1998.

646   Lohan, M. C., and Bruland, K. W.: The importance of vertical mixing for the supply of nitrate

647   and iron to the Columbia River plume: Implications for biology, Mar. Chem., 98, 260-273,

648   2006.

649   Lynn, R. J., and Simpson, J. J.: The California Current system: The seasonal variability of its

650   physical characteristics, J. Geophys. Res., 92(12), 12947-12966, 1987.

651 Martz, T., Send, U., Ohman, M. D., Takeshita, Y., Bresnahan, P., Kim, H.-J., and Nam, S. H.:

652   Dynamic variability of biogeochemical ratios in the Southern California Current System,

653   Geophys. Res. Lett., 41, 2496-2501, doi:10.1002/2014GL059332, 2014.

654 Oke, P. R., Allen, J. S., Miller, R. N., Egbert, G. D., Austin, J. A., Barth, J. A., Boyd, T. J., Kosro,

655   P. M., and Levine, M. D.: A modeling study of the three-dimensional continental shelf

656   circulation off Oregon. Part I: Model-data comparisons, J. Phys. Oceanogr., 32, 1360-1382,

657   2002.

658 Park, K.: Columbia River plume identification by specific alkalinity, Limnol. Oceanogr., 11, 118-

659   120, 1966.

660 Park, K.: Alkalinity and pH off the coast of Oregon, Deep-Sea Res., 15, 171-183, 1968.

661 Park, P. K., Catalfomo, M., Webster, G. R., and Reid, B. H.: Nutrients and carbon dioxide in the

662   Columbia river, Limnol. Oceanogr., 15, 70-79, 1970.

663 Park, P. K., Gordon, L. I., Hager, S. W., and Cissell, M. C.: Carbon dioxide partial pressure in the

664   Columbia river, Science, 166, 867-868, 1969a.

665 Park, P. K., Webster, G. R., and Yamamoto, R.: Alkalinity budget of the Columbia River, Limnol.

666   Oceanogr., 14, 559-567, 1969b.

667 Redfield, A. C., Ketchum, B. H., and Richards, F. A.: The influence of organisms on the

668   composition of seawater, in: The Sea, edited by M. N. Hill, Wiley, New York, 26-77, 1963.

669 Revelle, R., and Suess, H. E.: Carbon dioxide exchange between atmosphere and ocean and the

670   question of an increase of atmospheric CO_2 during the past decades, Tellus, 9, 18-27, 1957.

671 Sambrotto, R. M., Savidge, G., Robinson, C., Boyd, P., Takahashi, T., Karl, D. M., Langdon, C.,

672   Chipman, D., Marra, J., and Codispoti, L.: Elevated consumption of carbon relative to

nitrogen in the surface ocean, Nature, 363, 248-250, 1993.

Santana-Casiano, J. M., González-Dávila, M., and Ucha, I. R.: Carbon dioxide fluxes in the Benguela upwelling system during winter and spring: A comparison between 2005 and 2006, Deep-Sea Res. II, 56, 533-541, 2009.

Sigleo, A. C., and Frick, W. E.: Seasonal variations in river flow and nutrient concentrations in a northwestern USA watershed, in: First interagency conference on research in the watersheds, edited by K. G. Renard, S. A. McElroy, W. J. Gburek, H. E. Canfield, and R. L. Scott, U.S. Department of Agriculture, 370-376, 2003.

Snyder, M. A., Sloan, L. C., Diffenbaugh, N. S., and Bell, J. L.: Future climate change and upwelling in the California Current, Geophys. Res. Lett., 30(15), 1823, doi:10.1029/2003GL017647, 2003.

Spitz, Y. H., Allen, J. S., and Gan, J.: Modeling of ecosystem processes on the Oregon shelf during the 2001 summer upwelling, J. Geophys. Res., 110, C10S17, doi:10.1029/2005JC002870, 2005.

Sundquist, E. T., Plummer, L. N., and Wigley, T. M. L.: Carbon dioxide in the ocean surface: The homogenous buffer factor, Science, 204, 1203-1205, 1979.

Sydeman, W. J., García-Reyes, M., Schoeman, D. S., Rykaczewski, R. R., Thompson, S. A., Black, B. A., and Bograd, S. J.: Climate change and wind intensification in coastal upwelling ecosystems, Science, 345, 77-80, 2014.

Thomson, R. E., and Krassovski, M. V.: Poleward reach of the California Undercurrent extension, J. Geophys. Res., 115, C09027, doi:10.1029/2010JC006280, 2010.

Torres, R., Turner, D. R., Rutllant, J., and Lefèvre, N.: Continued CO_2 outgassing in an upwelling area off northern Chile during the development phase of El Niño 1997-1998 (July

696   1997), J. Geophys. Res., 108, 3336, doi:10.1029/2000JC000569, 2003.

697   Wetz, M. S., Hales, B., Chase, Z., Wheeler, P. A., and Whitney, M. M.: Riverine input of

698   macronutrients, iron, and organic matter to the coastal ocean off Oregon, U.S.A., during the

699   winter, Limnol. Oceanogr., 51, 2221-2231, 2006.

700   Wong, C. S., Waser, N. A. D., Nojiri, Y., Whitney, F. A., Page J. S., and Zeng, J.: Seasonal cycles

701   of nutrients and dissolved inorganic carbon at high and mid latitudes in the North Pacific

702   Ocean during the *Skaugran* cruises: determination of new production and nutrient uptake

703   ratios, Deep-Sea Res. II, 49, 5317-5338, 2002.

Table 1. $\Delta DIC - 6.6\Delta NO_3$, sea-air ΔpCO_2 and sea surface pCO_2 estimated with different DIC^{eff}, which is the combined freshwater end-member of

DIC partly sourced from the Columbia River (CR).

TAlk/DIC of CR (μmol kg^{-1})	NO$_3$ of CR (μmol kg^{-1})	DIC^{eff} (μmol kg^{-1})	$\Delta DIC - 6.6\Delta NO_3$ (μmol kg^{-1})		Sea-air ΔpCO_2 (μatm)		Sea surface pCO_2 (μatm)	
			Transect 4		Transect 4		Transect 4	
			Stations 27-32[a]	Station 33[b]	Stations 27-32[a]	Station 33[b]	Stations 27-32[a]	Station 33[b]
800	20	420	−25±3	−25±1	−60±6	−59±3	330±6	331±3
1000	15	450	−23±2	−23±1	−55±5	−53±3	335±5	337±3
1200	10	470	−22±2	−22±1	−53±5	−52±3	337±5	338±3
			Transect 5		Transect 5		Transect 5	
			Stations 35-38[b]		Stations 35-38[b]		Stations 35-38[b]	
800	20	540	−23±3		−53±8		337±8	
1000	15	585	−20±3		−48±8		342±8	
1200	10	610	−19±3		−46±8		344±8	
			Transect 6		Transect 6		Transect 6	
			Stations 45-49[b]		Stations 45-49[b]		Stations 45-49[b]	
800	20	500	−25±3		−57±6		333±6	
1000	15	540	−23±3		−53±6		337±6	
1200	10	570	−22±3		−51±6		339±6	

[a] data for these stations were obtained from waters immediately below the top buoyant layer.

[b] data for these stations were obtained from the surface mixed layer.

708 **Table 2.** $\Delta DIC - 6.6\Delta NO_3$, sea-air ΔpCO_2 and sea surface pCO_2 estimated with the deep water end-member from different depths.

Depth of the deep water end-member (m)	$\Delta DIC - 6.6\Delta NO_3$ ($\mu mol\ kg^{-1}$)		Sea-air ΔpCO_2 (μatm)		Sea surface pCO_2 (μatm)	
	Transect 4		Transect 4		Transect 4	
	Stations 27-32[a]	Station 33[b]	Stations 27-32[a]	Station 33[b]	Stations 27-32[a]	Station 33[b]
~130	−23±2	−19±1	−56±5	−45±3	334±5	345±3
~150	−23±2	−22±1	−55±5	−52±3	335±5	338±3
~175	−23±2	−23±1	−55±5	−53±3	335±5	337±3
~200	−23±2	−24±1	−55±5	−56±3	335±5	334±3
	Transect 5		Transect 5		Transect 5	
	Stations 35-38[b]		Stations 35-38[b]		Stations 35-38[b]	
~130	−21±3		−51±8		339±8	
~150	−20±3		−46±8		344±8	
~175	−20±3		−48±8		342±8	
~200	−17±3		−40±8		350±8	
	Transect 6		Transect 6		Transect 6	
	Stations 45-49[b]		Stations 45-49[b]		Stations 45-49[b]	
~130	−20±3		−46±6		344±6	
~150	−22±3		−51±6		339±6	
~175	−23±3		−53±6		337±6	
~200	−21±3		−50±6		340±6	

709 [a] data for these stations were obtained from waters immediately below the top buoyant layer.

710 [b] data for these stations were obtained from the surface mixed layer.

711 **Table 3.** Sea-air $\Delta p\mathrm{CO_2}$ and sea surface $p\mathrm{CO_2}$ estimated with different $\Delta\mathrm{DIC}-\mathrm{x}\Delta\mathrm{NO_3}$. x denotes the C/N uptake ratio during organic carbon

712 production. T and S represent transect and station(s).

C/N uptake ratio	$\Delta\mathrm{DIC}-\mathrm{x}\Delta\mathrm{NO_3}$ (µmol kg^{-1})				Sea-air $\Delta p\mathrm{CO_2}$ (µatm)				Sea surface $p\mathrm{CO_2}$ (µatm)			
	T4		T5	T6	T4		T5	T6	T4		T5	T6
	S27-32[a]	S33[b]	S35-38[b]	S45-49[b]	S27-32[a]	S33[b]	S35-38[b]	S45-49[b]	S27-32[a]	S33[b]	S35-38[b]	S45-49[b]
6.6[c]	−23±2	−23±1	−20±3	−23±3	−55±5	−53±3	−48±8	−53±6	335±5	337±3	342±8	337±6
7.3[d]	−42±3	−42±1	−39±3	−42±3	−101±6	−100±3	−92±8	−97±6	289±6	290±3	298±8	293±6

713 [a] data for these stations were obtained from waters immediately below the top buoyant layer.

714 [b] data for these stations were obtained from the surface mixed layer.

715 [c] 6.6 is the Redfield C/N uptake ratio (approximately 106/16; Redfield et al., 1963).

716 [d] 7.3 is the more recent evaluation of the C/N uptake ratio (approximately 117/16; Anderson and Sarmiento, 1994).

717
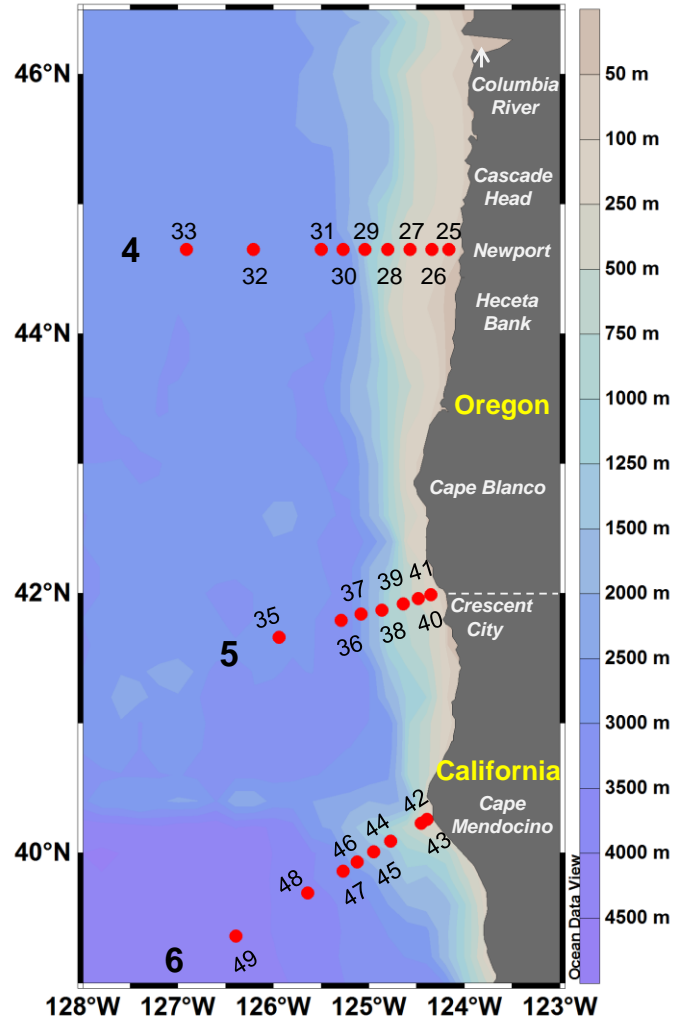
Fig. 1. Map of the US west coast off Oregon and northern California showing the topography and the locations of sampling stations along Transects 4, 5 and 6 in spring/early summer 2007.
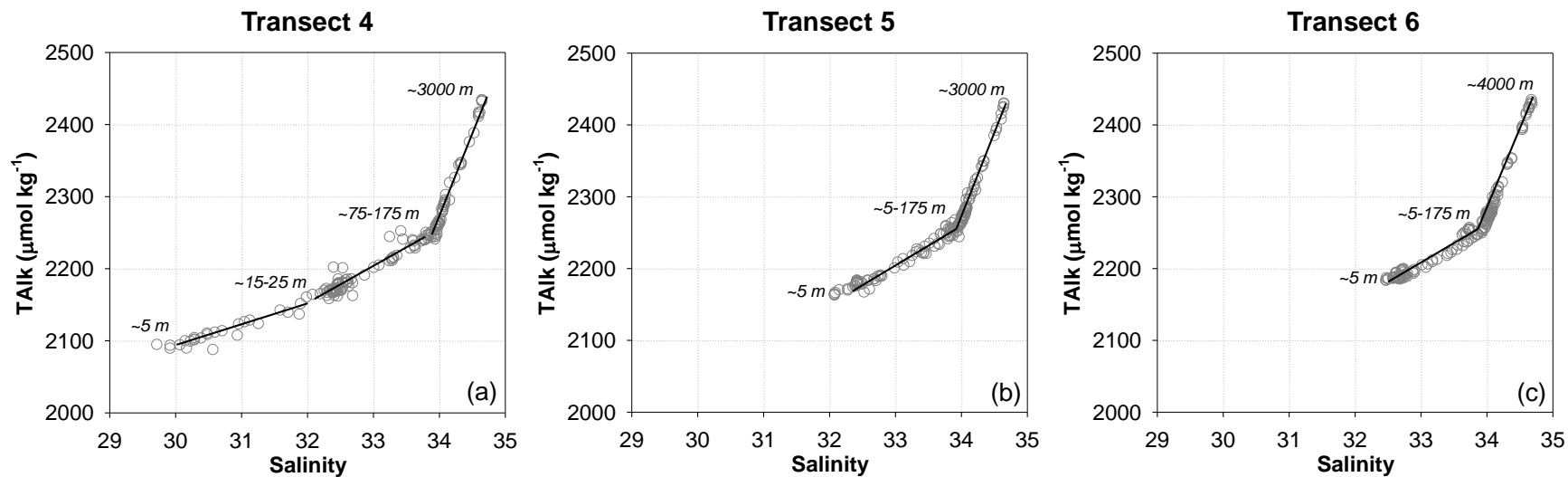
Fig. 2. Total alkalinity versus salinity through the entire water column of sampling stations along Transects 4 (a), 5 (b) and 6 (c) off Oregon and northern California in spring/early summer 2007. The solid lines indicate various linear relationships observed on each transect. The numbers in italics denote the sampling depth/depth range of the endpoints of each line.

724
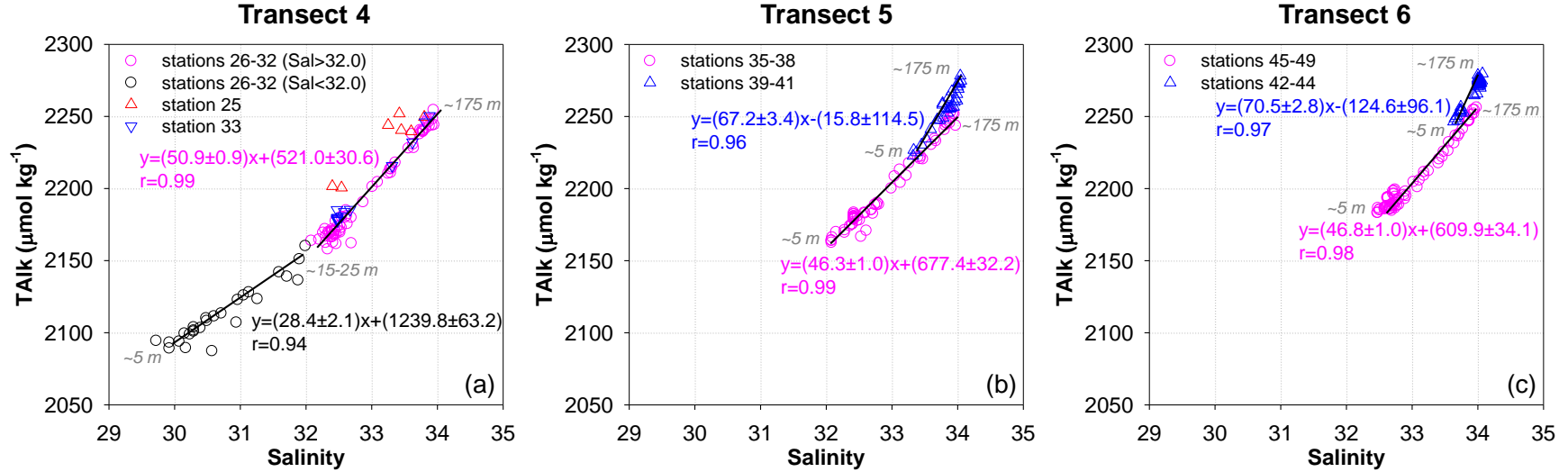
Fig. 3. Total alkalinity versus salinity (TAlk-Sal relationship) in the upper 175 m waters of sampling stations along Transects 4 (a), 5

(b) and 6 (c) off Oregon and northern California in spring/early summer 2007. The solid lines as well as the equations (in accordance

with the symbol colors) indicate the linear regression analyses of the TAlk-Sal relationship for various stations. The numbers in italics

denote the sampling depth/depth range of the endpoints of each line. In (a), the TAlk-Sal relationship at station 26-32 displayed two

phases for waters with salinity lower and higher than ~32.0. The top waters at these stations were imprinted by the Columbia River

plume. The data points of bottom waters at stations 26 (~75 m) and 27 (~130 m and ~160 m) were not included, as they were located

on the third linear relationship shown in Fig. 2a. In (b) and (c), stations 39-41 and stations 42-44 were largely influenced by coastal

upwelling.

733
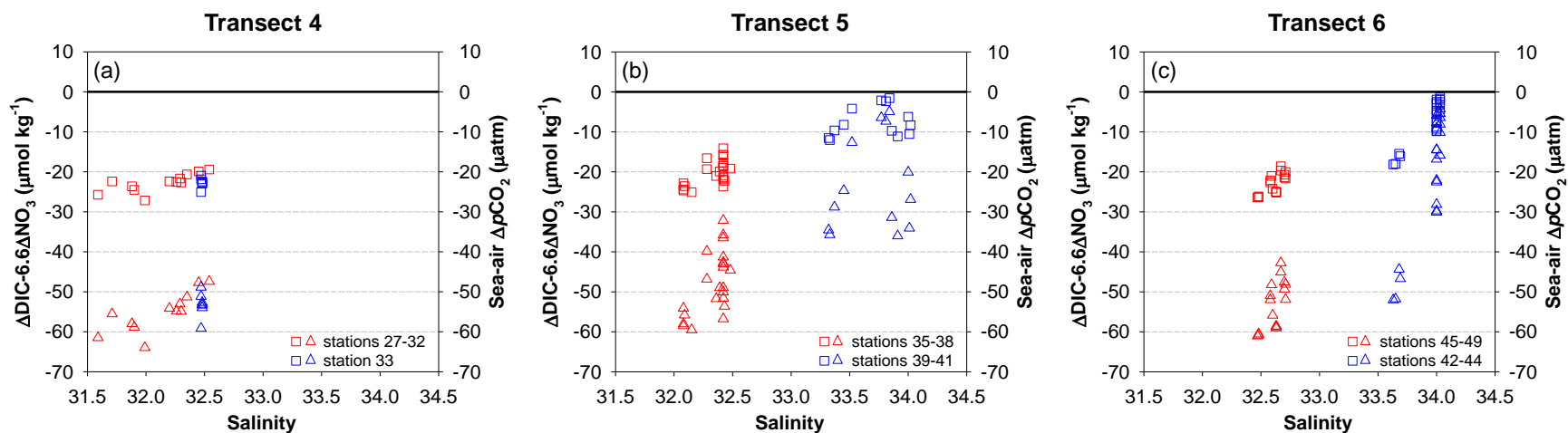
Fig. 4. ΔDIC-6.6ΔNO$_3$ (squares) and sea-air ΔpCO$_2$ (triangles) versus salinity in the upper waters on Transects 4 (a), 5 (b) and 6 (c)

off Oregon and northern California in spring/early summer 2007. Note that data for stations 27-32 on Transect 4 were obtained from

waters immediately below the top buoyant layer, while data for other stations were obtained from the surface mixed layer. The value

of 6.6 is the Redfield C/N uptake ratio (approximately 106/16; Redfield et al., 1963). The solid line indicates the pCO$_2$ equilibrium

between the seawater and the atmosphere.
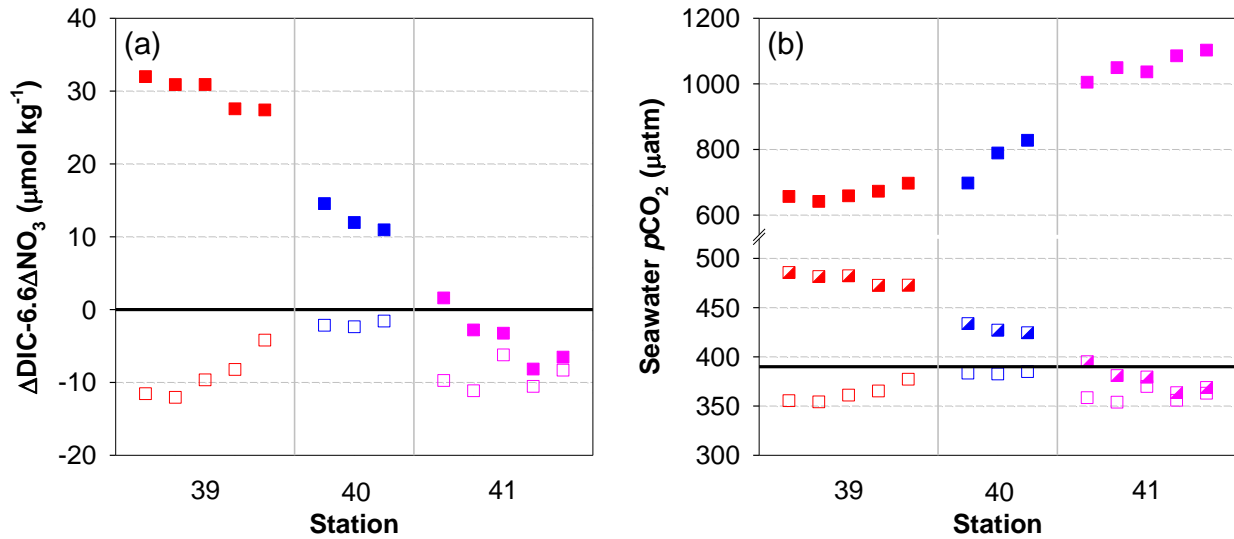
40

Fig. 5. $\Delta DIC - 6.6 \Delta NO_3$ (a) and seawater pCO_2 (b) in the surface mixed layer at stations 39-41 on Transect 5 near the Oregon-California border in spring/early summer 2007. In (a), open symbols indicate values estimated based on the two end-member mixing between the upwelling source water and the rainwater, while filled symbols indicate values after removing the rainwater. The value of 6.6 is the Redfield C/N uptake ratio (approximately 106/16; Redfield et al., 1963). The solid line indicates the pCO_2 equilibrium between the seawater and the atmosphere. In (b), the open and semi-filled symbols denote the estimated sea surface pCO_2 from $\Delta DIC - 6.6 \Delta NO_3$ on top of the mixing with and without rainwater, respectively. The filled symbols denote the field observed sea surface pCO_2, which were obtained by applying TAlk and DIC data into the CO2SYS program (Lewis and Wallace, 1998). The solid line denotes the atmospheric pCO_2 of ~390 μatm (Evans et al., 2011).

$$y=(6.70\pm0.37)x+(2000.0\pm0.7)$$
$$r=0.93$$

751
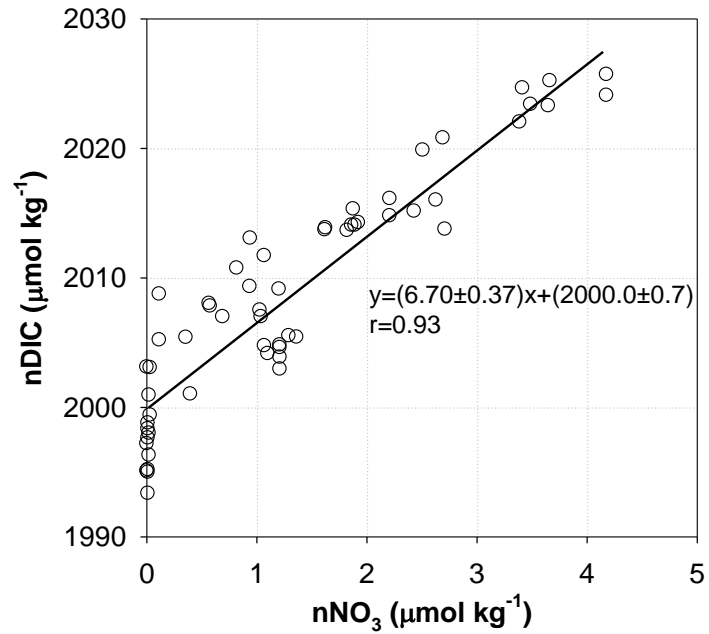
Fig. 6. Salinity normalized DIC (nDIC) versus salinity normalized NO_3 (nNO_3) in the CO_2 sink

zones off Oregon and northern California in spring/early summer 2007, which included waters

immediately below the top buoyant layer at stations 27-32 as well as waters in the surface mixed

layer at station 33 on Transect 4, waters in the surface mixed layer at stations 35-38 on Transect

5, and waters in the surface mixed layer at stations 45-49 on Transect 6.